Supporting Information

Covalent Organic Frameworks for Carbon Dioxide Capture from Air

Hao Lyu,[†] Haozhe Li,[†] Nikita Hanikel,[†] Kaiyu Wang,[†] Omar M. Yaghi[†,‡,*]

[†] Department of Chemistry and Kavli Energy Nanoscience Institute, University of California, Berkeley, California 94720, United States
[‡] KACST-UC Berkeley Joint Center of Excellence for Nanomaterials for Clean Energy Applications, King Abdulaziz City for Science and Technology, Riyadh 11442, Saudi Arabia

Table of Contents

Section S1 Materials and Methods

Chemicals Mesitylene (99%) and *n*-butanol (99.5%) were obtained from Acros Organics. Acetic acid (99.7%), diethyl ether (≥99.0 %, anhydrous) were purchased from Sigma Aldrich. Acetone (ACS grade), methanol (ACS grade), dichloromethane (DCM, ACS grade), ammonium chloride (NH_4Cl, ACS grade), and sodium sulfate (Na_2SO_4, anhydrous) were obtained from Fisher Scientific. 4,4'-Diaminobenzanilide (DABA, 98%) and tris(3-aminopropyl)amine (TRPN, 97%) were obtained from TCI America. 2,4,6-Tris-(4-bromophenyl)[1,3,5]triazine (95% for synthesis), *N*-formylpiperidine (99%), and 2-chloroethyl vinyl ether (97%, stabilized) were obtained from AK scientific. ^{15}N-labeled potassium phthalimide (98%) was purchased from Cambridge Isotope Laboratories. Dimethyl sulfoxide-d_6 (DMSO-d_6, 99.9 atom % D), deuterated chloroform ($CDCl_3$, 99.96 atom % D), carbonyl-^{13}C-labeled *N*,*N*-dimethylformamide (DMF-^{13}C, 99 atom %), and ^{13}C-labeled carbon dioxide ($^{13}CO_2$, 99 atom %) were obtained from Sigma Aldrich. All reagents were used without further purification, unless specified otherwise.

Nuclear Magnetic Resonance (NMR) Spectroscopy Solution ^1H NMR spectra were acquired on a Bruker AV-600 (600 MHz), a Bruker AV-500 (500 MHz), or a Bruker Avance NEO 500 (500 MHz) spectrometer at 297–300 K. Chemical shifts were calculated using the solvent resonances as internal standards (δ ^1H: 2.50 ppm for DMSO-d_6, 7.26 ppm for $CDCl_3$; δ ^{13}C: 39.52 ppm for DMSO-d_6, 77.16 ppm for $CDCl_3$). A polynomial baseline correction was applied to each spectrum before integration using Mestrelab MestReNova software.

Solid-state ^{13}C and ^{15}N NMR experiments were conducted on a Bruker AV-500 (500 MHz) or a Bruker Avance NEO 400 (400 MHz) spectrometer at 297–300 K. All samples were fully activated, packed, and sealed in zirconia rotors in an argon-filled glovebox before loading into the probe for measurements.

Experiments on AV-500 spectrometer were performed using a Bruker 4-mm double resonance MAS probe (^1H/X) operating at 125.75 MHz for ^{13}C and at 50.69 MHz for ^{15}N, and a magic angle spinning rate of 8 kHz. Experiments on the NEO 400 spectrometer were performed using a 3.2-mm or 1.3-mm MAS probe (^1H/X) operating at 100.65 MHz for ^{13}C and at 50.69 MHz for ^{15}N, and a magic angle spinning rate of 24 kHz. The magic angle was calibrated by maximizing the number and intensity of rotational echoes for the ^{79}Br resonance for KBr under MAS. ^{13}C chemical shifts were externally referenced to the downfield resonance of adamantane at 38.48 ppm. ^{15}N chemical shifts were externally referenced to glycine at 33.4 ppm.

^{13}C multiple cross polarization (multi-CP) experiments were performed using the compensated-multi-CP (compMulti-CP) sequence developed by Schmidt Rohr and coworkers using a ^1H 90° pulse time of 5.0 μs, a ^{15}N 90° pulse time of 5.0 μs, 50 contact periods of 50 μs, an inter-contact delay of 1.0 s, a relaxation delay of 6 s, and 70 kHz two pulse phase modulated (TPPM) ^1H decoupling during acquisition. Due to the significant difference of ^{13}C abundance between ^{13}C-labeled and unlabeled compounds, signals from unlabeled carbon were neglected during integration of signals of labeled ^{13}C in different chemical environments.

High-Resolution Mass Spectrometry (HRMS) Electron ionization and electrospray ionization HRMS measurements were performed at the QB3/Chemistry Mass Spectrometry Facility at University of California, Berkeley.

Fourier-Transform Infrared Spectroscopy (FT-IR) Attenuated total reflectance Fourier-transform infrared spectroscopy (ATR-FT-IR) of solid samples were performed on a Bruker ALPHA Platinum ATRFT-IR spectrometer equipped with a single reflection diamond ATR module. All spectra were collected on activated samples neat in ambient atmosphere, if not specified otherwise. The signals are given in transmittance (%) against wavenumbers (cm^{-1}).

Powder X-ray diffraction (PXRD) PXRD patterns were collected using a Rigaku Miniflex 600 X-ray diffractometer in reflection geometry employing Cu Kα lines (λ = 1.54184 Å, with a Ni filter) at a power of 600 W (40 kV, 15 mA). Samples were mounted on Si (511) sample holders and leveled with a spatula.

Scanning electron microscopy (SEM) Scanning electron micrographs were recorded on an FEI Quanta 3D FEG scanning electron microscope with an accelerating voltage of 15 kV and a working distance of 10.8 mm. Powder samples were casted on a carbon tape on a stainless steel holder. Energy Dispersive X-ray spectroscopy (EDS) data were collected using an Oxford X-Max EDS system working at an acceleration voltage of 15 kV.

Elemental microanalysis (EA) Combustion EA measurements on fully activated samples were performed using a Perkin Elmer 2400 Series II CHNS elemental analyzer at the Microanalytical Laboratory of the College of Chemistry, University of California, Berkeley.

Single-Component Sorption Isotherm Measurements Powder samples were activated under a dynamic vacuum using a Micromeritics ASAP2420 Accelerated Surface Area and Porosimetry System. Supercritical CO_2 drying was performed on a tousimis Samdri-PVT-3D critical point dryer. Nitrogen (N_2) sorption isotherms were measured using a Micromeritics ASAP2420 Accelerated Surface Area and Porosimetry System. A liquid nitrogen bath was used to maintain a temperature of 77 K for each measurement. Ultra-high-purity (Praxair, 99.999%) N_2 and helium (He) gases were used throughout the adsorption experiments.

CO_2 sorption isotherms were measured using a Micromeritics 3Flex Adsorption Analyzer. A water circulation bath was used to maintain a temperature of 25.00 °C for each measurement except as otherwise specified. Research-grade CO_2 (Praxair, 99.998%) was used throughout the adsorption experiments.

H_2O vapor sorption isotherms were measured using a BEL Japan BELSORP-aqua^3 high precision vapor adsorption instrument. The water vapor source was degassed through five freeze-pump-thaw cycles before the analysis. Ultra-high-purity grade He was used for free space corrections and an isothermal bath was employed to adjust the sample temperature during the measurements.

Section S2. Synthesis

S2.1 Synthesis of Molecular Compounds

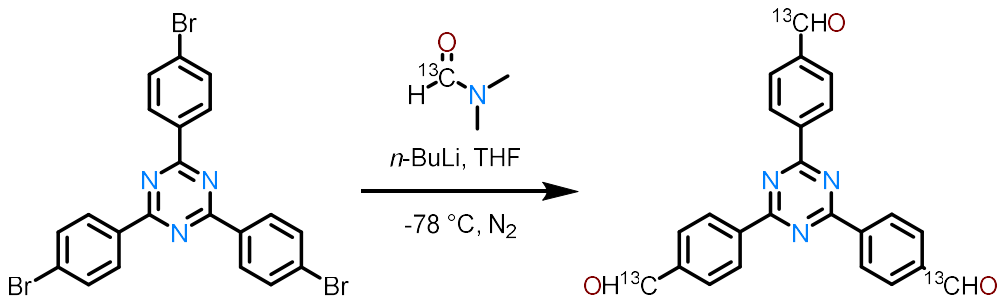

Synthesis of 2,4,6-tris(4-formylphenyl)-1,3,5-triazine (TFPT) was performed according to a reported procedure[1]. ^{13}C-labelled TFPT (termed as TFPT-^{13}C) was obtained based on a reported procedure[2]. A suspension of 2,4,6-tris-(4-bromophenyl)-1,3,5-triazine (0.885 g, 1.82 mmol) in tetrahydrofuran (THF, 90 mL, HPLC grade, purified through an Inert PureSolv Solvent Purification System) was cooled to –78 °C under an inert atmosphere, to which was charged *n*-butyllithium solution (2.6 mL, 6.5 mmol, 2.5 mol L^{-1} in hexanes) dropwise over 10 mins. After stirring for 90 mins at –78 °C, to the reaction mixture was added DMF-^{13}C (1.0 mL) at –78 °C, which was kept for 15 mins and allowed to warm to 20–25 °C. The mixture was kept stirring for 1 h. The reaction was quenched with 45 mL saturated aqueous NH_4Cl solution and stirred for 1 h. The organic volatiles were partially removed by evaporation under reduced pressure, and the remaining mixture was extracted between 200 mL water and 200 mL dichloromethane. The organic phase was collected, and the aqueous phase was washed with dichloromethane twice (100 mL each). The combined organic phase was dried over anhydrous sodium sulfate, filtered, and evaporated to dryness under reduced pressure. The solid was subjected to flash column chromatography using silica gel and DCM with 0–1% methanol as eluent. The collected fractions were evaporated to dryness and recrystallized in methanol to yielding the product TFPT-^{13}C (0.296 g, yield 33%). ^{1}H NMR (600 MHz, $CDCl_3$) δ 10.19 (d, J = 175.7 Hz, 3H), 8.96 (m, 6H), 8.13 (m, 6H). ^{13}C NMR (151 MHz, $CDCl_3$) δ 191.80, 171.31, 140.78, 139.34 (d, J = 53.1 Hz), 129.82 (dd, J = 42.2, 4.2 Hz). HRMS (EI^+) for $[^{12}C_{21}{}^{13}C_3H_{15}N_3O_3]^+$ (M^+): m/z Calcd. 396.1214, Found 396.1217.

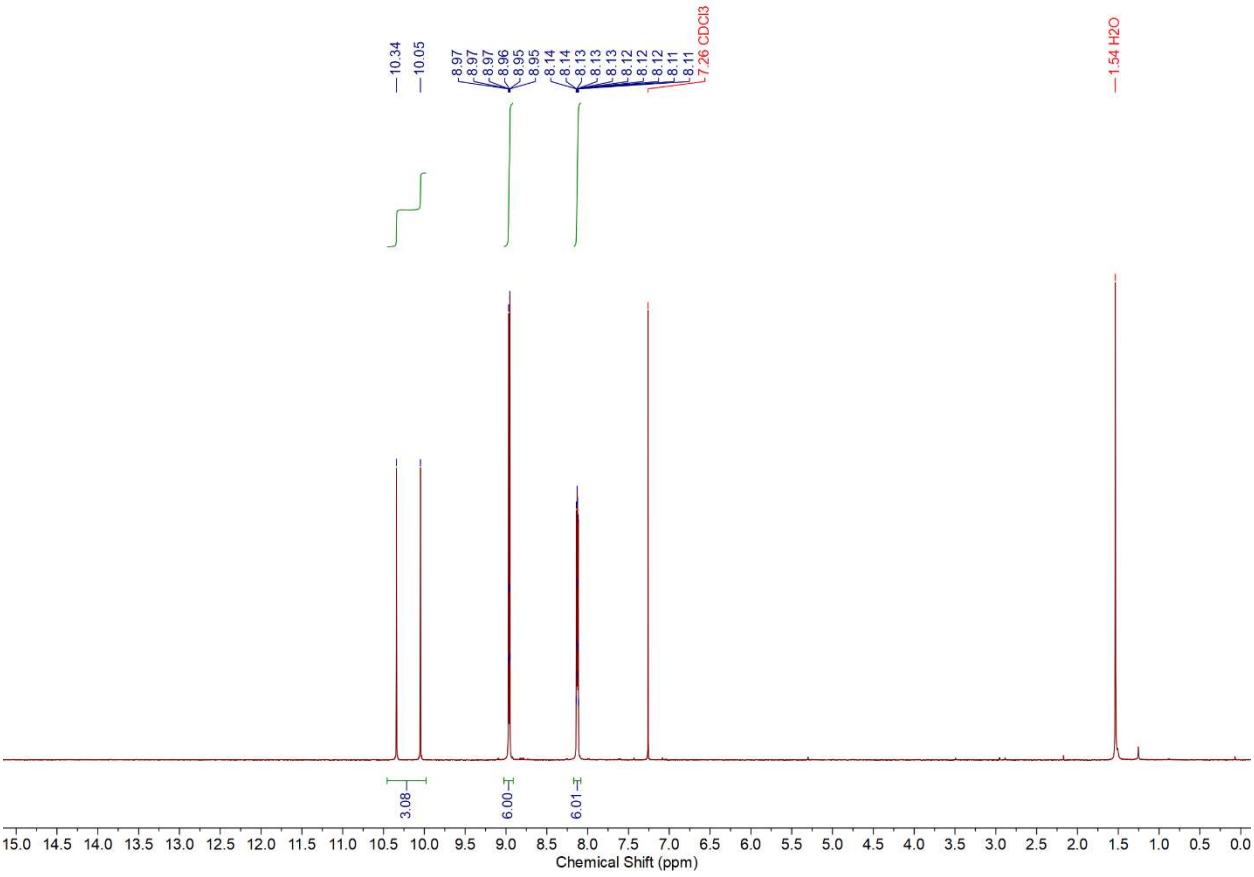

Figure S1. ^{1}H NMR spectrum of TFPT-^{13}C in $CDCl_3$.

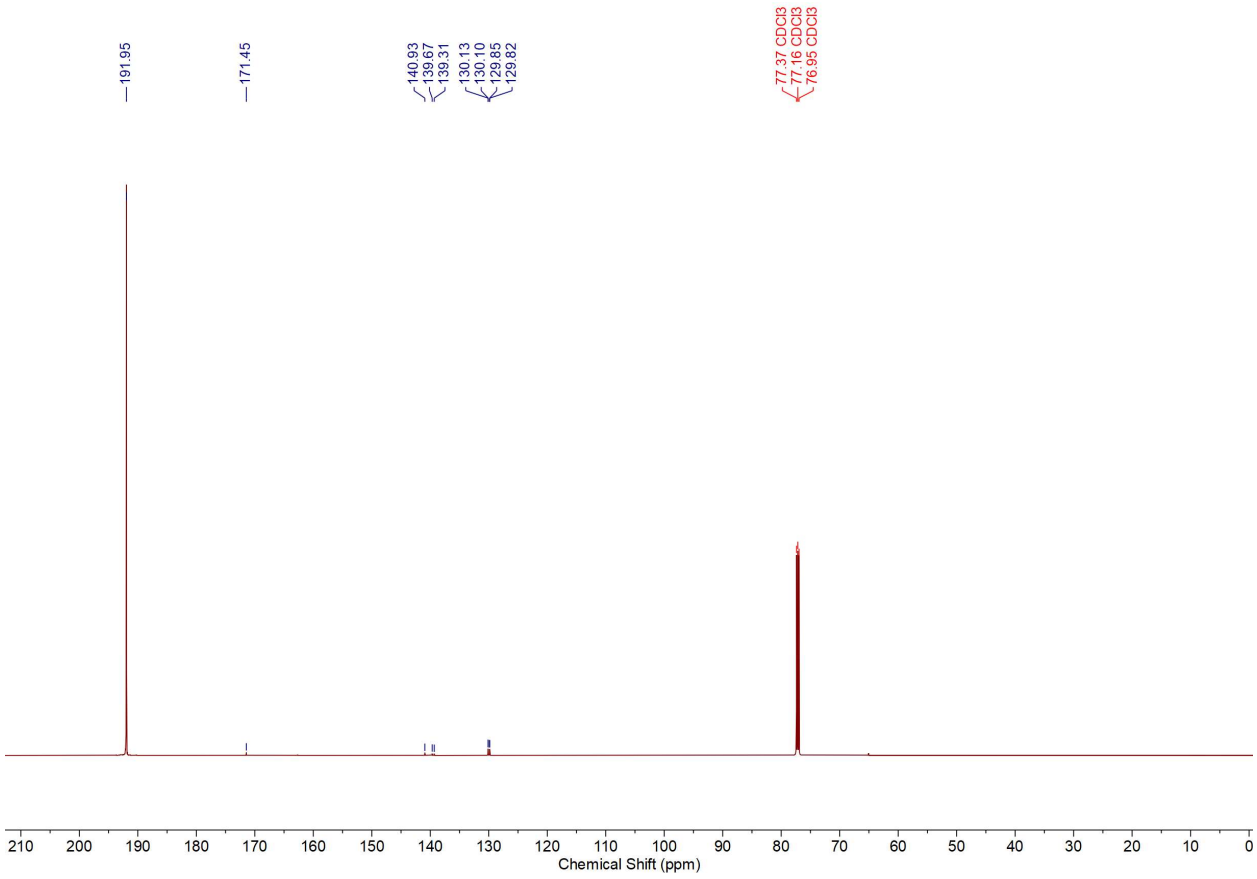

Fig. S2. ^{13}C NMR spectrum of TFPT-^{13}C in $CDCl_3$.

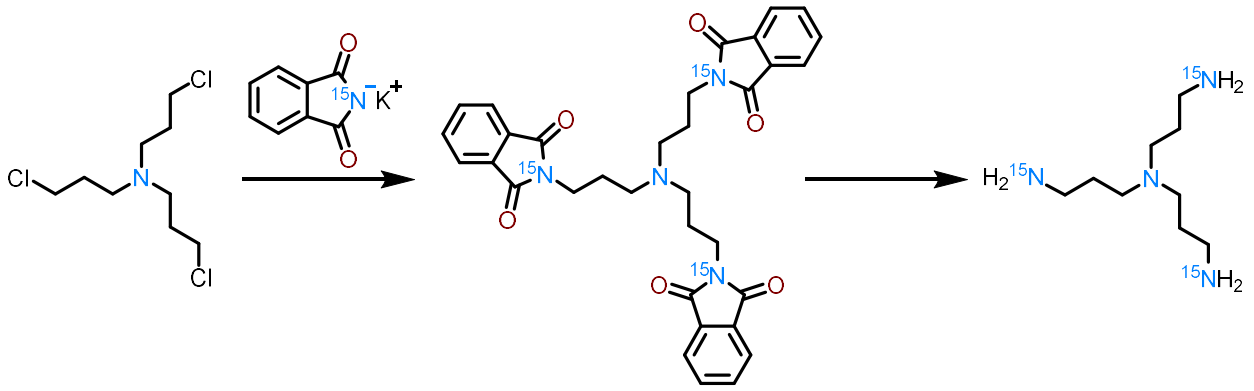

Synthesis of ^{15}N-labeled tris(3-aminopropyl)amine (TRPN-^{15}N) was achieved using Gabriel synthesis by reacting tris(3-chloropropyl)amine, obtained following a reported procedure[3], with ^{15}N-labeled potassium phthalimide followed by cleaving the product with hydrazine. In the first step, tris(3-chloropropyl)amine (1.246 g, 5.05 mmol) was mixed with potassium phthalimide-^{15}N (3.103 g, 16.7 mmol) in 6 mL DMF and heated to reflux for 3 h. The solvent was first removed using a rotary evaporator, and the mixture was washed with water, followed by washing with a 1:1 mixture of hexanes and ethyl acetate. The white precipitation was collected as the product (1.086 g, yield 37%). ^{1}H NMR (500 MHz, DMSO) δ 7.81 (q, *J* = 1.2 Hz, 12H), 3.59 (t, *J* = 7.2 Hz, 6H), 2.40 (t, *J* = 6.9 Hz, 6H), 1.67 (p, *J* = 7.3 Hz, 6H). ^{13}C NMR (151 MHz, DMSO) δ 167.84 (d, *J* = 13.2 Hz), 134.23, 131.65 (d, *J* = 7.4 Hz), 122.89, 50.62, 35.79 (d, *J* = 9.4 Hz), 25.38. ^{15}N NMR (61 MHz, DMSO) δ 162.74. HRMS (ESI^{+}) for $[^{12}C_{33}H_{31}N^{15}N_3O_6]^{+}$ (M+H^{+}): m/z Calcd. 582.2149, Found 582.2145.

The product, 2,2',2''-(nitrilotris(propane-3,1-diyl))tris(isoindoline-1,3-dione-^{15}*N*) (0.780 g, 1.35 mmol) was further treated with hydrazine monohydrate (204 μL, 4.185 mmol) in 3 mL ethanol and refluxed for 2 h, according to a reported procedure [4]. The reaction was cooled down and was made strongly acidic using concentrated hydrochloric acid. The solids formed was repetitively washed with ethanol and filtered off. The combined filtrate was collected and evaporated under reduced pressure. The residue was treated with a 40% NaOH solution and extracted with chloroform. The organic layer was collected, dried over Na_2SO_4, and evaporated to dryness. The residue was dried at room temperature using a Schlenk line (0.05 Torr) equipped with a liquid nitrogen cold trap to collect the product as a light-yellow oil (0.298 g, yield 86%).^{1}H NMR (500 MHz, DMSO) δ 2.52 (t, *J* = 6.6 Hz, 6H), 2.34 (t, *J* = 7.1 Hz, 6H), 2.21 (br), 1.43 (pd, *J* = 6.9, 2.0 Hz, 6H). ^{13}C NMR (126 MHz, DMSO) δ 51.40, 48.58, 30.72. ^{15}N NMR (61 MHz, DMSO) δ 33.28. HRMS (ESI^{+}) for $[^{12}C_9H_{25}N^{15}N_3]^{+}$ (M+H^{+}): m/z Calcd. 192.1985, Found 192.1981.

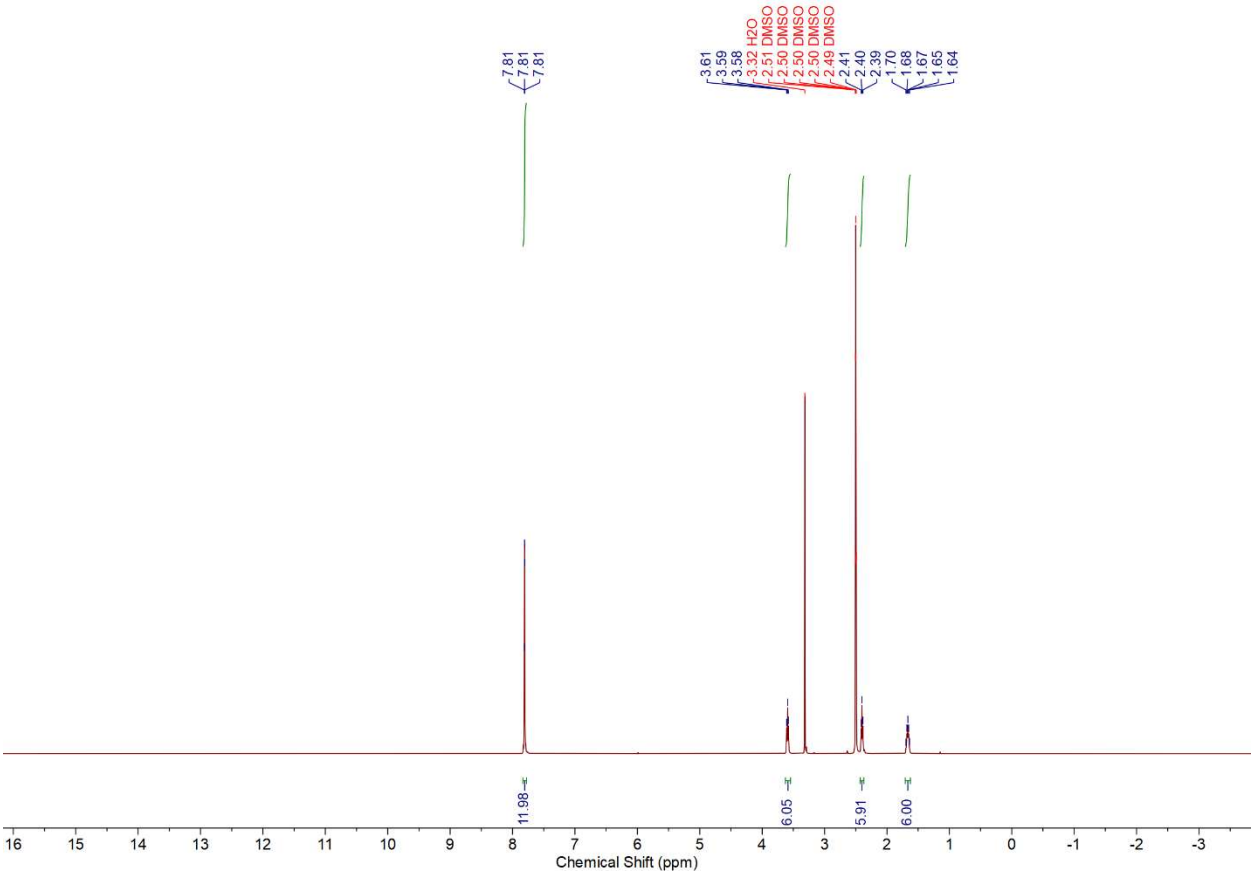

Fig. S3. ^{1}H NMR spectrum of 2,2',2''-(nitrilotris(propane-3,1-diyl))tris(isoindoline-1,3-dione-^{15}N) in DMSO-d_6.

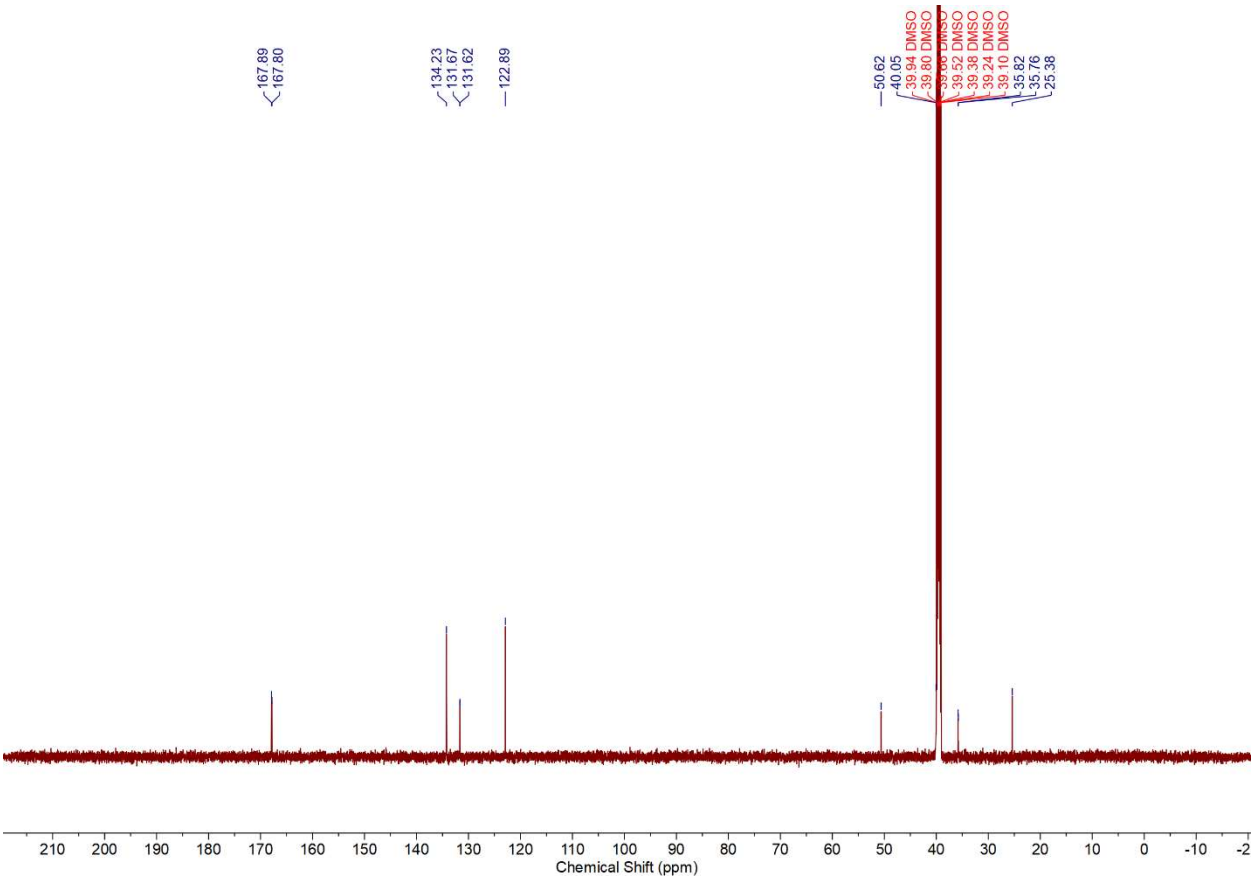

Fig. S4. ^{13}C NMR spectrum of 2,2',2''-(nitrilotris(propane-3,1-diyl))tris(isoindoline-1,3-dione-^{15}N) in DMSO-d_6.

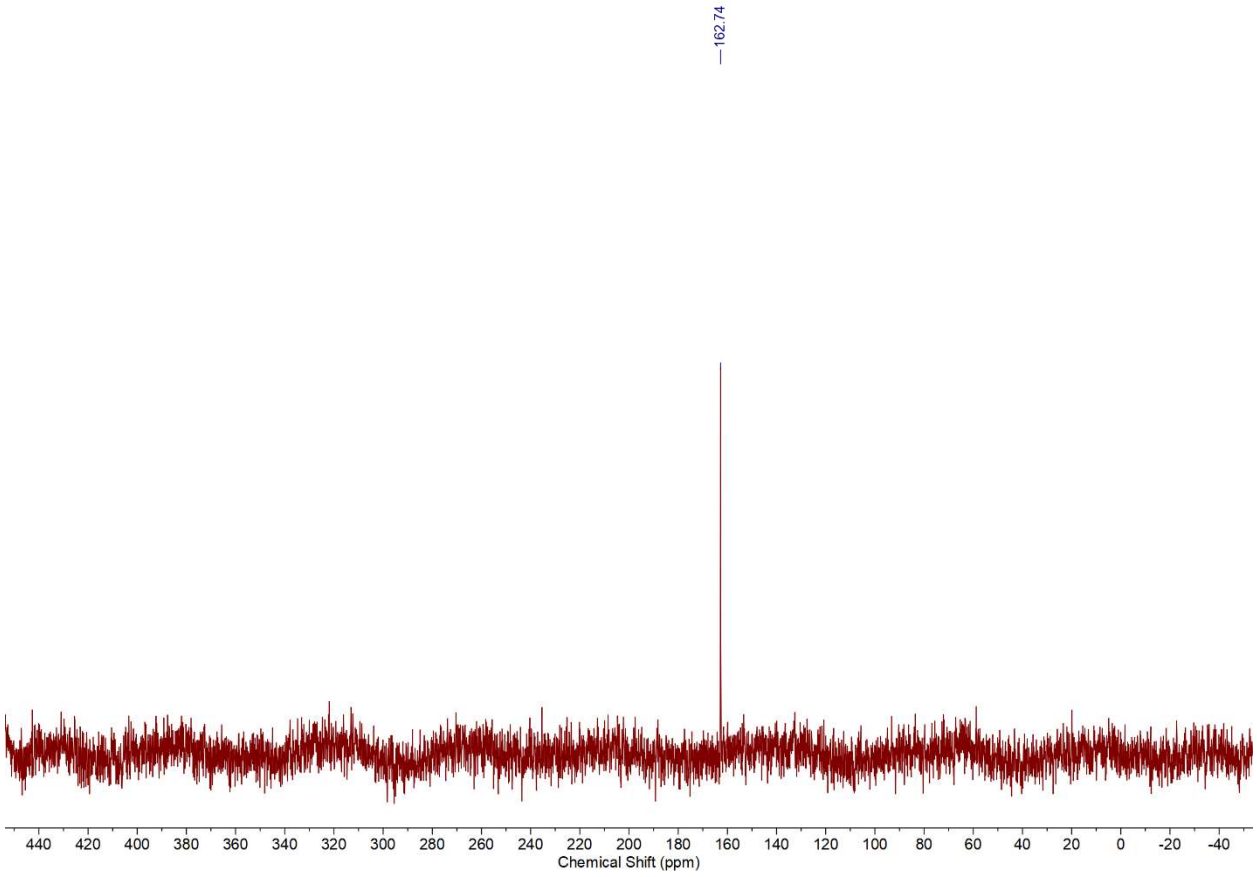

Fig. S5. ^{15}N NMR spectrum of 2,2',2''-(nitrilotris(propane-3,1-diyl))tris(isoindoline-1,3-dione-^{15}N) in DMSO-d_6.

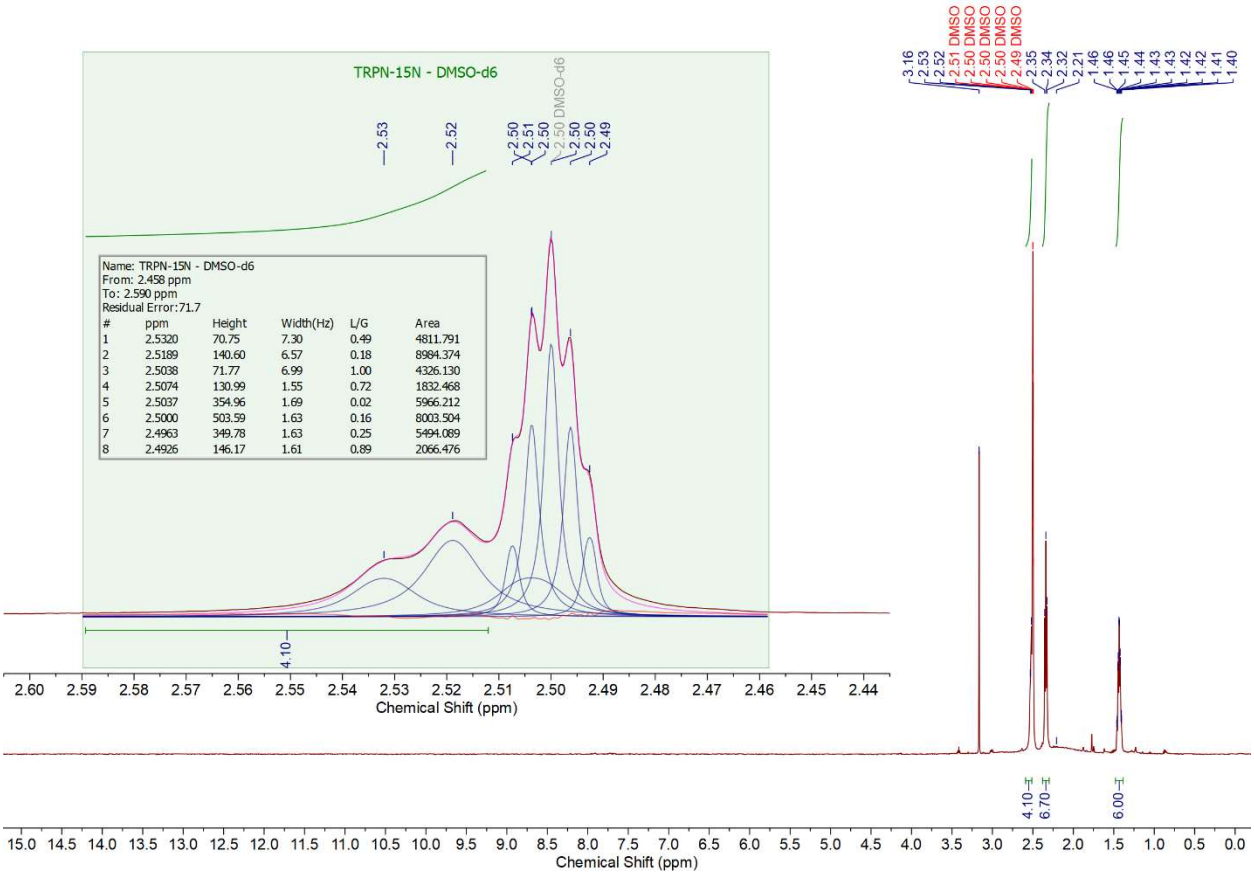

Fig. S6. ^{1}H NMR spectrum of TRPN-^{15}N in DMSO-d_6. Due to peak overlapping, the integration of the triplet signal at 2.34 ppm deviated above the actual value. Part of the triplet at 2.52 ppm overlaps with the residual DMSO solvent peak at 2.50 ppm, rendering missing assignments of peaks and an integration underrepresenting the actual value. Inset shows the result of linear deconvolution of the overlapping region (2.458–2.590 ppm) using MestReNova, which supported the presence of a triplet at 2.52 ppm (TRPN-^{15}N) and a quintet at 2.50 ppm (DMSO-d_6) that showed good agreement with the experimental spectrum. Similarly, the broad peak at 2.21 ppm was not integrated due to overlapping with other signals. Color code for lines: experimental data, maroon; simulated peak profiles, blue; sum of simulated signals, violet; simulation-experiment difference, red.

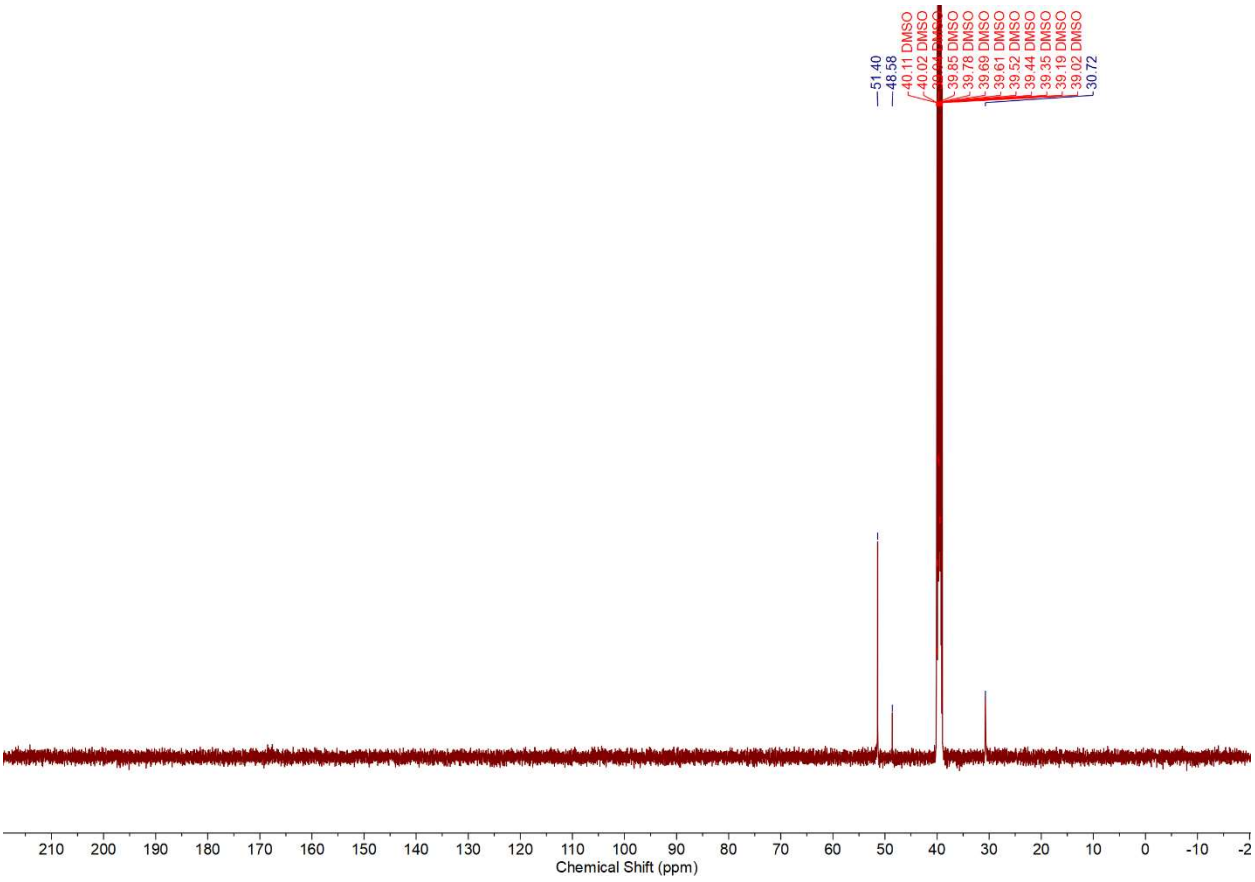

Fig. S7. ^{13}C NMR spectrum of TRPN-^{15}N in DMSO-d_6.

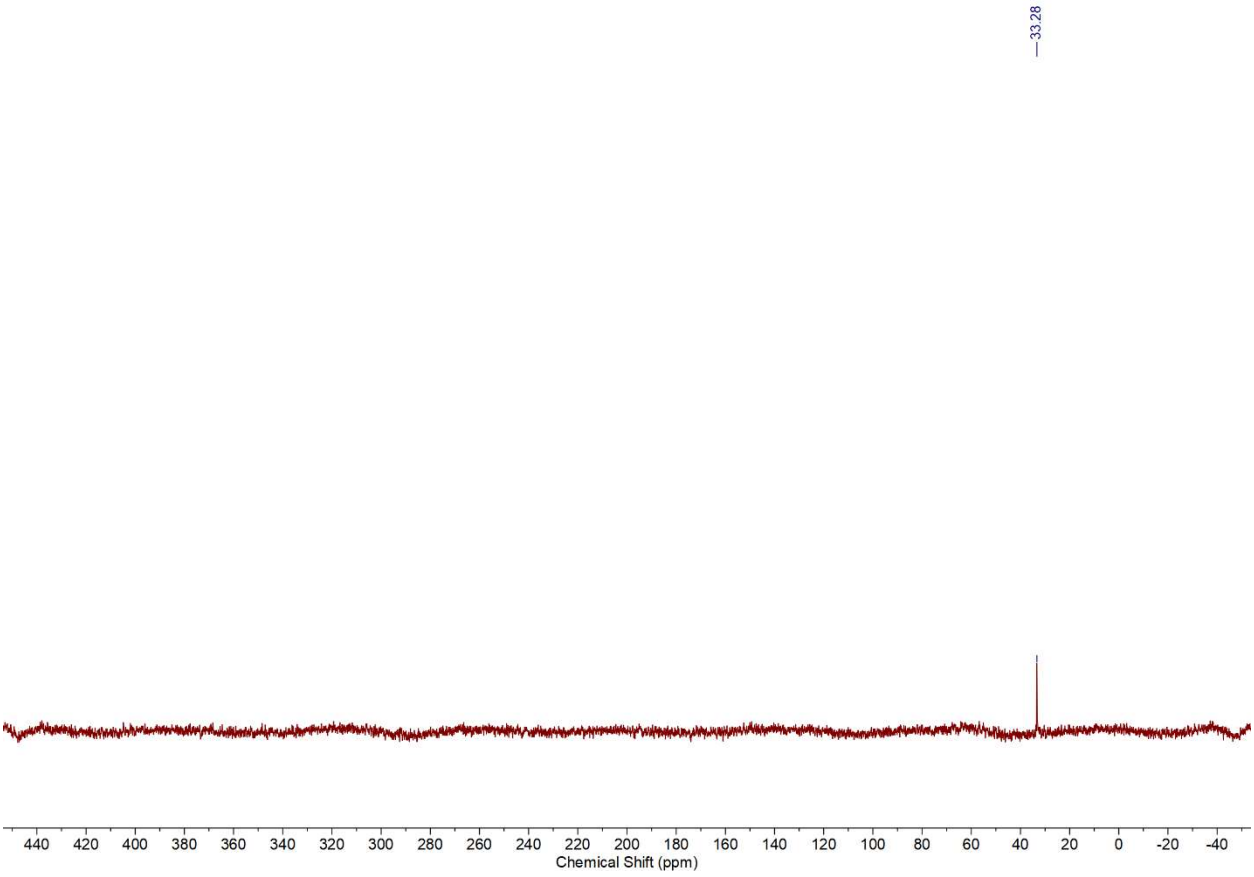

Fig. S8. ^{15}N NMR spectrum of TRPN-^{15}N in DMSO-d_6.

S2.2 Crystallization of COF-609-Im

Synthesis of COF-609-Im was performed in a borosilicate glass tube measuring 8×10 mm (i.d. × o.d.), where TFPT (15.7 mg, 0.04 mmol) and DABA (13.6 mg, 0.06 mmol) are mixed in 0.85 mL mesitylene and 0.15 mL *n*-butanol. The mixture was sonicated for 5 minutes before introducing 0.05 mL acetic acid solution (9 mol L^{-1} in deionized water). The obtained suspension was further sonicated for 5 minutes and was flash frozen at 77 K in a liquid nitrogen bath, evacuated to an internal pressure below 150 mTorr, and flame sealed. The length of the tube was reduced to around 10 cm upon sealing. After warming to room temperature, the reaction was heated at 140 °C for 4 days to yield a yellow solid. The solid was collected, washed with acetone and methanol for 1 day in a Soxhlet extractor, dried with supercritical CO_2, and degassed at 140 °C for 24 h to yield COF-609-Im as a yellow-colored solid (yield 67%). Elemental analysis for $C_{29}H_{19}N_5O$: Calcd. C 76.81%, H 4.22%, N 15.44%; Found C 76.36%, H 4.61%, N 15.34%.

S2.3 Post-Synthetic Modification

Conversion of the imine linkage in COF-609-Im was performed by mixing COF-609-Im (136.2 mg, 0.6 mmol by imine linkage), anhydrous $FeCl_3$ (12 mg, 0.072 mmol), as well as 2-chloroethyl vinyl ether (0.90 mL, 8.8 mmol) in diethyl ether (12 mL) under an inert atmosphere, in a 20 mL glass vial equipped with an open-top screw cap with a PTFE/silicone septum. The vial was kept still at 50 °C for 2 days. After cooling to room temperature, the supernatant was decanted and the solid was washed with methanol and acetone in a Soxhlet extractor for 1 day. The solid was collected, washed with acetone and methanol for 1 day in a Soxhlet extractor, dried with supercritical CO_2, and degassed at 140 °C for 24 h to yield COF-609-THQ,Im as a dark-yellow solid (187.8 mg, apparent yield 94%). Elemental analysis for $C_{37}H_{33}N_5O_3Cl_2$: Calcd. C 66.67%, H 4.99%, N 10.51%; Found C 66.98%, H 5.01%, N 10.27%.

Activated powders of COF-609-THQ,Im (131 mg) were immersed in 2.0 mL TRPN under argon in a 4 mL glass vial sealed by an open-top screw cap with a PTFE/silicone septum. The reaction was heated to 140 °C for 24 h before cooling down to room temperature, and washed repetitively with methanol, acetone, and dichloromethane for 1 day. The sample was further treated with a 10 wt % potassium hydroxide solution in methanol for 1 day, and washed repetitively with methanol and acetone for 1 day before activation under a dynamic vacuum at 140 °C for 24 h. The product was obtained as brown powders. Elemental analysis for $C_{55}H_{79}N_{13}O_3$: Calcd. C 68.08%, H 8.21%, N 18.77%; Found C 69.48%, H 7.98%, N 15.58%.

Section S3. Fourier-Transform Infrared Spectroscopy

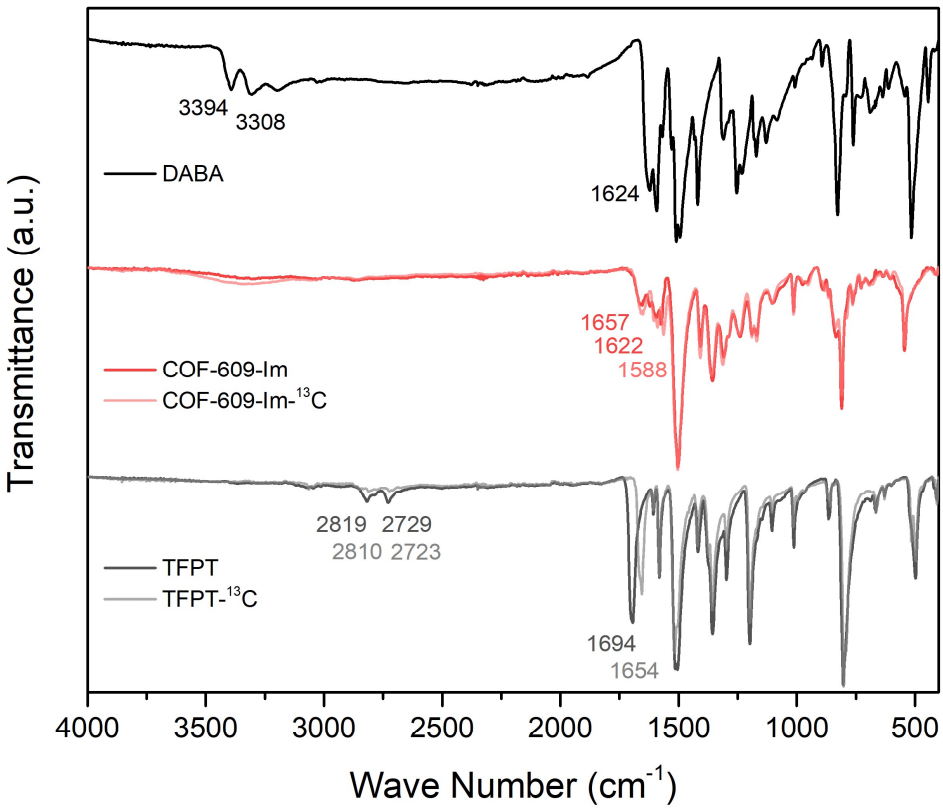

Fig. S9. Stacked FT-IR spectra of DABA, COF-609-Im, COF-609-Im-^{13}C, TFPT, and TFPT-^{13}C.

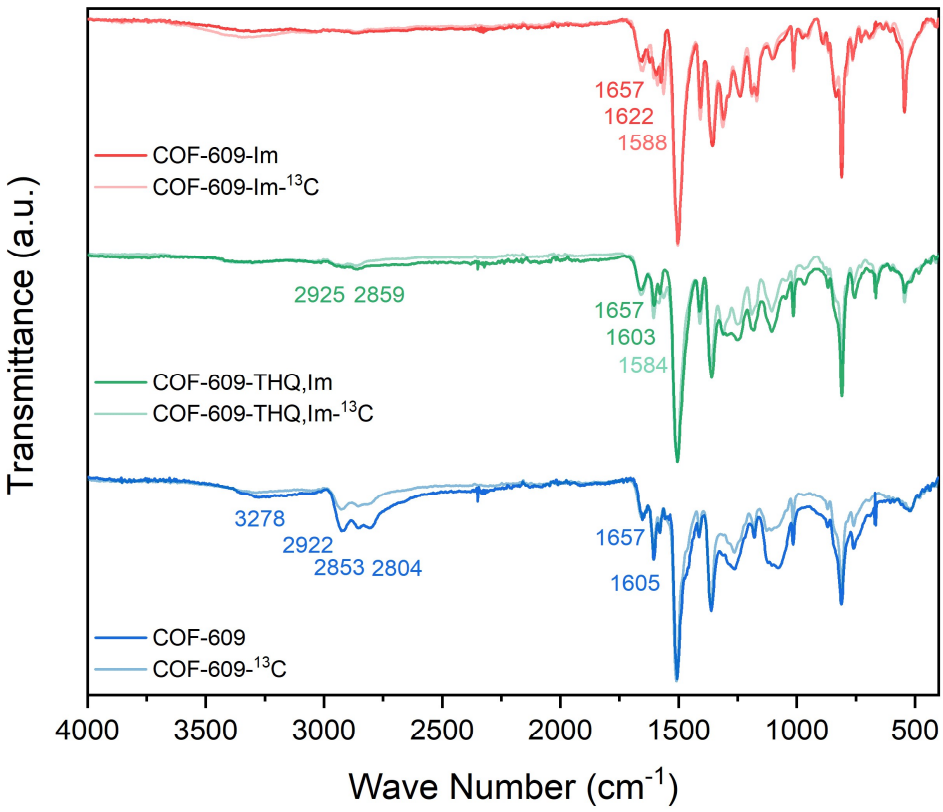

Figure S10. Full-range stacked FT-IR spectra of COF-609-Im, COF-609-Im-^{13}C, COF-609-THQ,Im, COF-609-THQ,Im-^{13}C, COF-609, and COF-609-^{13}C.

General procedure for FT-IR vibrational analysis using isotope effects. In the vibrational analysis of bonds with isotope labeled and unlabeled atoms, the FT-IR absorbance of relevant vibration normal modes displays differences such as wavenumber shifts, known as the isotope effect.[5] For stretching vibrations, simple quantitative analysis is carried out by treating the bond stretches as simple harmonic oscillators, of which the wavenumber of absorbance $\tilde{\nu}$ can be given by the following equation:

$$\tilde{\nu} = \frac{1}{2\pi c}\sqrt{\frac{k}{\mu}}$$

where c is the speed of light in vacuum, k is the force constant of the bond vibration mode, and μ is the reduced mass of bond A-B, given by the equation:

$$\mu = \sqrt{\frac{m_A m_B}{m_A + m_B}}$$

where m_i is the mass of atom i (i = A, B) in bond A-B. The correlation between the wavenumber of absorbance $\tilde{\nu}$ and the mass of atoms in bond A-B can be established by the expression:

$$\tilde{\nu} \propto \sqrt{\frac{1}{\mu}} = \sqrt{\frac{m_A + m_B}{m_A m_B}}$$

As such, with a measured wavenumber $\tilde{\nu}$ of a vibration of interest, the expected wavenumber of the same stretching mode with different isotopes can be estimated by the above expression, and therefore yield useful information by comparison with values from experimental data measured on correspondent samples.

Table S1. Selected FT-IR Absorbance Compared to Estimation Calculated by Simple Harmonic Oscillator Model

Compound	Vibration (major component)		Absorbance (cm^{-1})		
	Non-labeled	Labeled	Non-labeled	Calculated	Observed
TFPT	$^{12}C{=}^{16}O$	$^{13}C{=}^{16}O$	1694	1656	1654
	$^{12}C{=}^{1}H$	$^{13}C{=}^{1}H$	2819 2729	2811 2721	2810 2723
COF-609-Im	$^{12}C{=}^{14}N$	$^{13}C{=}^{14}N$	1622	1588	1588

Section S4. Powder X-Ray Diffraction

Structural elucidation of COF-609-Im was performed by comparing the experimental PXRD pattern with proposed atomic model built in *BIOVIA* Materials Studio[6] and relaxed through geometric optimization with the *Forcite* module using Universal forcefield. The model was used to simulate a PXRD pattern and compared with the experimental result, which showed good agreement in terms of reflection positions and relative intensities. Pawley refinement was thus performed on this atomic model against the experimental pattern (Figure S11). The obtained unit cell and atomic coordinates are provided in Table S2. As only a single Bragg diffraction was observed in COF-609-THQ,Im and no Bragg peaks in COF-609, we only provide unit cell and atomic coordinates of geometrically optimized models in Table S3 and S4.

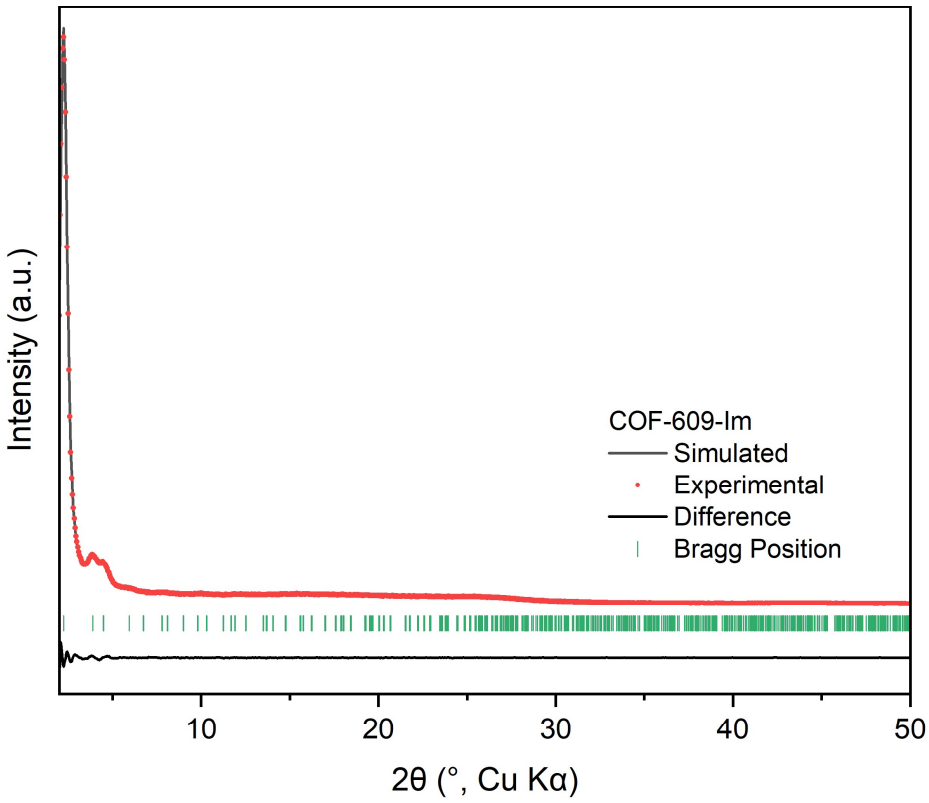

Figure S11. Pawley refinement result for the PXRD pattern of COF-609-Im. Agreement factors: R_{wp} = 2.19%, R_p = 1.70 %.

Table S2. Fractional Atomic Coordinates of Structural Model of COF-609-Im, Resulting from Pawley Refinement

COF-609-Im			
Hexagonal, *P*3 $a = b = 45.6580$ Å, $c = 3.4766$ Å $\alpha = \beta = 90$ °, $\gamma = 120$ °			
Atom	***x***	***y***	***z***
N1	0.36556	0.68221	0.81028
C2	0.34900	0.64985	0.81033
C3	0.36603	0.63158	0.80866
C4	0.39950	0.64742	0.82222
C5	0.41555	0.63019	0.81907
C6	0.39845	0.59675	0.80165
C7	0.36509	0.58090	0.78844
C8	0.34901	0.59810	0.79226
C9	0.41486	0.57802	0.79542
N10	0.44573	0.59199	0.81535
C11	0.46389	0.57599	0.80913
C12	0.49704	0.59402	0.84315
C13	0.57552	0.48082	0.98038
H14	0.50863	0.61964	0.87532
H15	0.41338	0.67317	0.83551
H16	0.44134	0.64308	0.82954
H17	0.35141	0.55513	0.77469
H18	0.32323	0.58512	0.78108
C19	0.52671	0.48302	0.90583
C20	0.55951	0.49810	0.98698
C21	0.51010	0.45017	0.83367
H22	0.48472	0.43800	0.77807
H23	0.57268	0.52299	1.06664
H24	0.53526	0.15664	0.85149
C25	0.52089	0.53064	0.7874
N26	0.63477	0.32144	0.86352
C27	0.65468	0.35349	0.8635
C28	0.64166	0.37540	0.86436
C29	0.60858	0.36337	0.87827
C30	0.59631	0.38403	0.88035
C31	0.61687	0.41718	0.86793
C32	0.64986	0.42922	0.85339
C33	0.66216	0.40858	0.85189
C34	0.60450	0.43950	0.87055
N35	0.57405	0.42898	0.88669
C36	0.55891	0.44800	0.89524

C37	0.52607	0.43287	0.82783
C38	0.44933	0.54285	0.76564
H39	0.51285	0.40757	0.76780
H40	0.59209	0.33796	0.88849
H41	0.57073	0.37403	0.89183
H42	0.66617	0.45469	0.84353
H43	0.68775	0.41869	0.84057
C44	0.50092	0.54592	0.79802
C45	0.46758	0.52790	0.75936
C46	0.51545	0.57919	0.83677
H47	0.54107	0.59372	0.86549
H48	0.45548	0.50242	0.71484
H49	0.44769	0.84834	0.77397
N50	0.50935	0.49997	0.91703
O51	0.54786	0.54578	0.65829
H52	0.48608	0.48729	1.02206
H53	0.60056	0.49316	1.05215
H54	0.42068	0.52721	0.73342

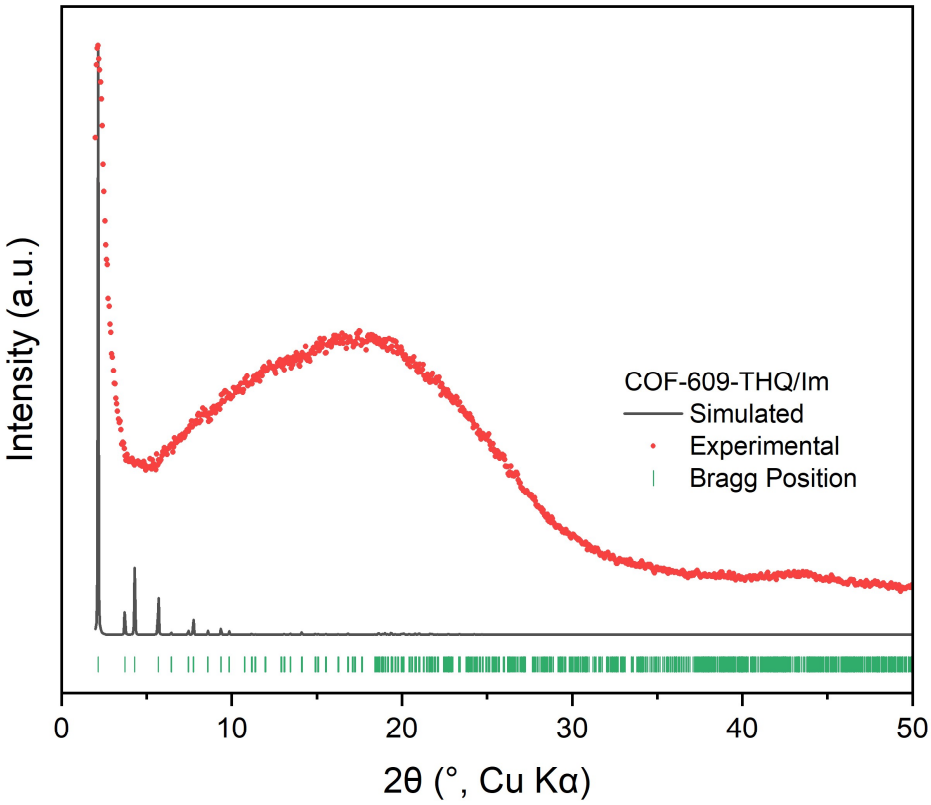

Figure S12. Comparison of experimental PXRD pattern of COF-609-Im with simulated PXRD pattern of COF-609-THQ (assuming 100% THQ linkage in COF-609-THQ,Im).

Table S3. Fractional Atomic Coordinates of Structural Model of COF-609-THQ (Assuming 100% THQ Linkage in COF-609-THQ,Im), Resulting from Geometric Optimization

COF-609-THQ (Assuming 100% THQ Linkage in COF-609-THQ,Im)			
Hexagonal, *P*3 $a = b = 45.5200$ Å, $c = 4.7944$ Å $\alpha = \beta = 90$ °, $\gamma = 120$ °			
Atom	***x***	***y***	***z***
N1	0.36536	0.67609	0.16139
C2	0.34281	0.64395	0.16276
C3	0.35314	0.61959	0.12864
C4	0.38309	0.62536	0.23497
C5	0.39436	0.60389	0.17576
C6	0.37617	0.57667	0.00450
C7	0.34582	0.57049	0.90489
C8	0.33427	0.59159	0.96839
C9	0.38957	0.55511	0.91556
N10	0.42280	0.57464	0.81097
C11	0.44357	0.56087	0.78703
C12	0.47244	0.57726	0.63378
C13	0.55562	0.46384	0.80797
H14	0.47947	0.60056	0.53944
H15	0.39801	0.64675	0.35978
H16	0.41786	0.60917	0.25410
H17	0.33131	0.54967	0.77280
H18	0.31124	0.58677	0.88152
C19	0.50936	0.46887	0.65140
C20	0.53780	0.48015	0.81121
C21	0.49814	0.44034	0.49511
H22	0.47612	0.43119	0.37281
H23	0.54614	0.50160	0.93992
H24	0.58465	0.15353	0.09790
C25	0.50381	0.51816	0.66448
N26	0.63372	0.31669	0.79056
C27	0.64998	0.34968	0.78968
C28	0.63204	0.36738	0.80582
C29	0.60689	0.35802	0.00030
C30	0.59117	0.37604	0.02921
C31	0.59976	0.40326	0.85940
C32	0.62392	0.41158	0.65480
C33	0.64048	0.39426	0.63328
C34	0.58248	0.42256	0.89765
N35	0.55909	0.41558	0.67438

C36	0.54335	0.43452	0.65628
C37	0.51499	0.42328	0.49744
C38	0.43445	0.53044	0.90908
H39	0.50567	0.40100	0.37864
H40	0.60014	0.33738	0.13614
H41	0.57233	0.36874	0.18549
H42	0.63030	0.43155	0.51282
H43	0.65951	0.40149	0.47883
C44	0.48298	0.53282	0.70840
C45	0.45435	0.51669	0.86744
C46	0.49199	0.56340	0.59490
H47	0.51394	0.57637	0.47175
H48	0.44777	0.49354	0.96095
H49	0.46126	0.83546	0.74540
N50	0.49057	0.48499	0.65818
O51	0.53290	0.53598	0.62689
H52	0.46536	0.47031	0.64197
C53	0.38924	0.53384	0.15615
C54	0.40206	0.51143	0.06033
O55	0.40528	0.49576	0.30053
C56	0.39241	0.46192	0.25979
C57	0.35860	0.44225	0.38892
Cl58	0.32868	0.44582	0.19279
H59	0.42978	0.59694	0.71514
H60	0.36414	0.51898	0.23884
H61	0.40506	0.54976	0.32448
H62	0.40868	0.45511	0.37032
H63	0.39207	0.45469	0.03816
H64	0.35871	0.45033	0.60572
H65	0.35160	0.41619	0.39425
C66	0.60598	0.45937	0.90923
C67	0.58789	0.47857	0.96331
O68	0.60607	0.51172	0.87870
C69	0.63853	0.52902	0.97685
C70	0.64127	0.53373	0.29089
Cl71	0.68271	0.56103	0.37878
H72	0.38413	0.49432	0.90660
H73	0.58218	0.47733	0.18940
H74	0.64964	0.55363	0.88343
H75	0.65332	0.51837	0.90279
H76	0.63354	0.51023	0.39521
H77	0.62598	0.54393	0.36247
H78	0.61893	0.46748	0.70719

H79	0.62407	0.46464	0.07731
H80	0.54923	0.39343	0.56819

Table S4. Fractional Atomic Coordinates of Structural Model of COF-609, Resulting from Geometric Optimization

COF-609			
Hexagonal, *P*3 $a = b = 46.5335$ Å, $c = 4.7830$ Å $\alpha = \beta = 90$ °, $\gamma = 120$ °			
Atom	***x***	***y***	***z***
N1	0.36637	0.67786	0.90273
C2	0.34459	0.64469	0.90409
C3	0.35684	0.62116	0.86827
C4	0.38869	0.62936	0.96066
C5	0.40176	0.60887	0.89609
C6	0.38343	0.58015	0.73387
C7	0.35118	0.57142	0.64964
C8	0.33789	0.59158	0.71816
C9	0.39875	0.55988	0.63605
N10	0.43208	0.58163	0.52389
C11	0.45636	0.57126	0.51239
C12	0.48593	0.59024	0.36513
C13	0.59492	0.49694	0.57423
H14	0.49045	0.61263	0.25903
C15	0.40030	0.53859	0.87385
H16	0.40375	0.65198	0.07741
H17	0.42675	0.61619	0.96176
H18	0.33654	0.54939	0.52486
H19	0.31338	0.58481	0.64217
C20	0.62954	0.51515	0.69516
C21	0.54269	0.49485	0.46210
C22	0.57434	0.51102	0.58718
C23	0.53182	0.46433	0.32902
H24	0.50739	0.45139	0.23693
H25	0.58283	0.53407	0.69943
H26	0.42155	0.50785	0.96755
O27	0.39706	0.49529	0.57355
C28	0.37835	0.46307	0.68777
C29	0.39714	0.44384	0.65867
H30	0.35506	0.44991	0.56438
H31	0.37018	0.46304	0.90719
H32	0.41965	0.45803	0.52723
H33	0.38064	0.41998	0.55012
N34	0.40647	0.43747	0.93528
C35	0.41650	0.41210	0.92569
H36	0.42600	0.45957	0.01516

C37	0.45089	0.42505	0.79070
H38	0.39751	0.38984	0.81247
H39	0.41710	0.40429	0.14396
H40	0.44943	0.42792	0.56164
C41	0.46583	0.40266	0.84744
H42	0.46821	0.45000	0.87778
H43	0.49286	0.41819	0.80325
N44	0.45084	0.37286	0.66615
H45	0.46354	0.39582	0.07213
C46	0.47547	0.36447	0.55421
C47	0.42135	0.34397	0.78931
H48	0.42712	0.32520	0.87276
C49	0.39418	0.32767	0.56665
H50	0.41155	0.35149	0.96861
H51	0.40295	0.31713	0.40104
H52	0.38966	0.34667	0.46782
C53	0.36156	0.29960	0.68553
H54	0.36626	0.28307	0.82285
H55	0.34593	0.28444	0.50764
N56	0.34364	0.31294	0.83862
H57	0.35469	0.32099	0.03461
H58	0.31965	0.29333	0.87688
H59	0.46292	0.34278	0.41155
C60	0.49469	0.35718	0.78043
H61	0.49349	0.38547	0.42372
C62	0.52278	0.35354	0.64844
H63	0.47782	0.33387	0.89269
H64	0.50574	0.37757	0.93549
H65	0.51254	0.33408	0.48369
N66	0.53978	0.34450	0.85759
H67	0.54109	0.37734	0.54889
H68	0.52273	0.32162	0.94505
H69	0.54830	0.36213	0.01809
H70	0.66632	0.50366	0.86659
H71	0.62402	0.47531	0.96017
H72	0.51767	0.17252	0.38016
H73	0.57149	0.16636	0.32384
C74	0.52954	0.54075	0.46758
N75	0.63578	0.32936	0.80780
C76	0.66267	0.36039	0.80914
C77	0.65820	0.38943	0.77536
C78	0.62910	0.38831	0.86991
C79	0.62303	0.41410	0.80681

C80	0.64567	0.44121	0.64475
C81	0.67530	0.44287	0.55866
C82	0.68165	0.41733	0.62537
C83	0.63726	0.46706	0.54765
N84	0.60357	0.45083	0.43231
C85	0.58347	0.46622	0.43900
C86	0.55211	0.45030	0.31473
C87	0.45038	0.54180	0.64555
H88	0.54338	0.42691	0.20780
C89	0.64039	0.49032	0.78769
H90	0.61072	0.36713	0.98692
H91	0.59994	0.41224	0.87282
H92	0.69315	0.46350	0.43347
H93	0.70417	0.41869	0.54797
C94	0.41711	0.51902	0.77753
C95	0.50427	0.55122	0.48622
C96	0.47454	0.53221	0.63497
C97	0.50963	0.58031	0.35130
H98	0.53189	0.59510	0.23093
H99	0.46997	0.50992	0.74361
H100	0.62883	0.52875	0.88487
O101	0.65133	0.53660	0.48604
C102	0.67778	0.56578	0.60346
C103	0.66820	0.59286	0.63391
H104	0.69912	0.57489	0.45716
H105	0.68690	0.56105	0.80418
H106	0.64219	0.58318	0.56350
H107	0.68477	0.61411	0.49796
N108	0.67226	0.60451	0.92357
C109	0.66188	0.62944	0.95971
H110	0.65810	0.58421	0.05394
C111	0.62405	0.61342	0.99701
H112	0.67032	0.64712	0.78091
H113	0.67452	0.64428	0.14861
H114	0.61125	0.60313	0.79491
C115	0.61450	0.63834	0.10770
H116	0.61512	0.59267	0.14904
H117	0.58784	0.62454	0.16422
N118	0.62167	0.66413	0.89439
H119	0.62798	0.64895	0.30732
C120	0.59121	0.65968	0.75495
C121	0.64460	0.69799	0.99910
H122	0.63228	0.70578	0.15600

C123	0.65913	0.72342	0.76041
H124	0.66576	0.69784	0.10541
H125	0.63896	0.72547	0.65562
H126	0.67099	0.71501	0.60380
C127	0.68457	0.75817	0.86486
H128	0.67379	0.76603	0.03613
H129	0.69066	0.77586	0.68824
N130	0.71494	0.75922	0.95931
H131	0.71140	0.75050	0.16507
H132	0.73364	0.78412	0.96855
H133	0.59809	0.67326	0.55385
C134	0.57105	0.67133	0.92923
H135	0.57509	0.63307	0.69835
C136	0.53755	0.66091	0.78923
H137	0.58514	0.69880	0.94747
H138	0.56640	0.66039	0.14151
H139	0.54145	0.66803	0.56525
N140	0.52054	0.67655	0.92197
H141	0.52154	0.63354	0.80225
H142	0.53537	0.70231	0.90353
H143	0.51765	0.67078	0.13485
H144	0.37491	0.52118	0.95238
H145	0.41503	0.55508	0.04691
H146	0.45711	0.84029	0.46640
H147	0.39660	0.83355	0.42042
N148	0.52031	0.50772	0.47833
O149	0.55852	0.56179	0.43169
H150	0.49503	0.49023	0.46844

Section S5. Thermogravimetric Analyses

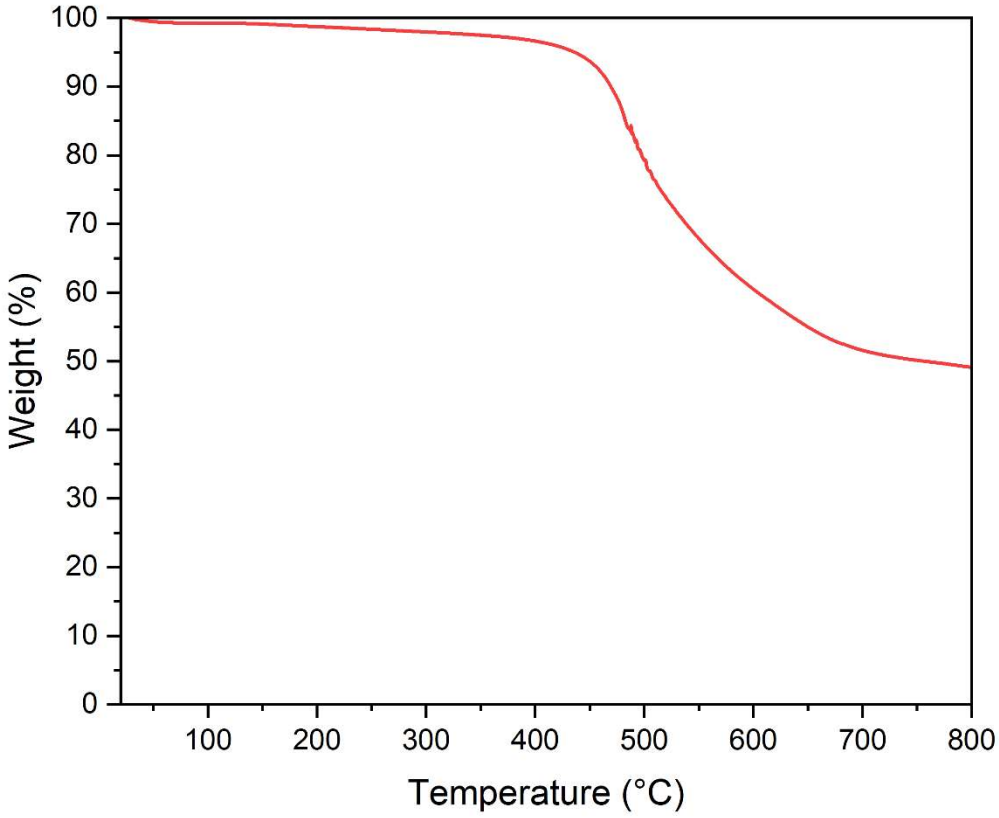

Fig. S13. TGA trace of COF-609-Im measured under a continuous flow of N_2. No significant weight loss was observed up to around 400 °C.

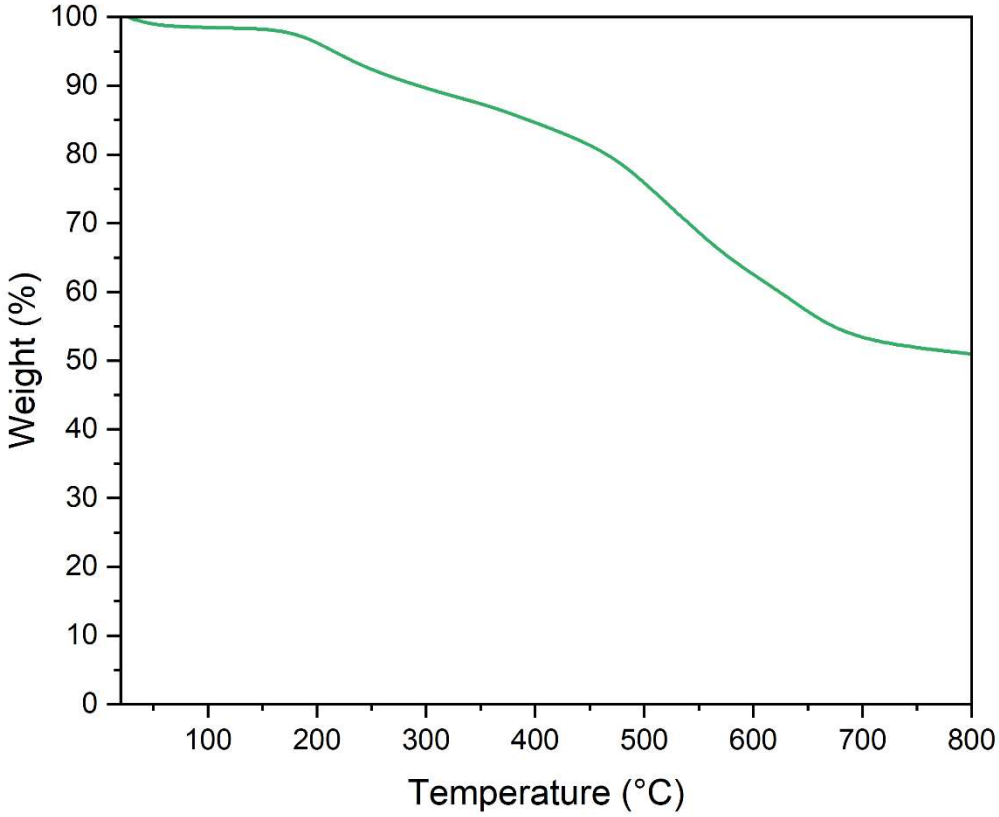

Fig. S14. TGA trace of COF-609-THQ,Im measured under a continuous flow of N_2. No significant weight loss was observed up to around 180 °C.

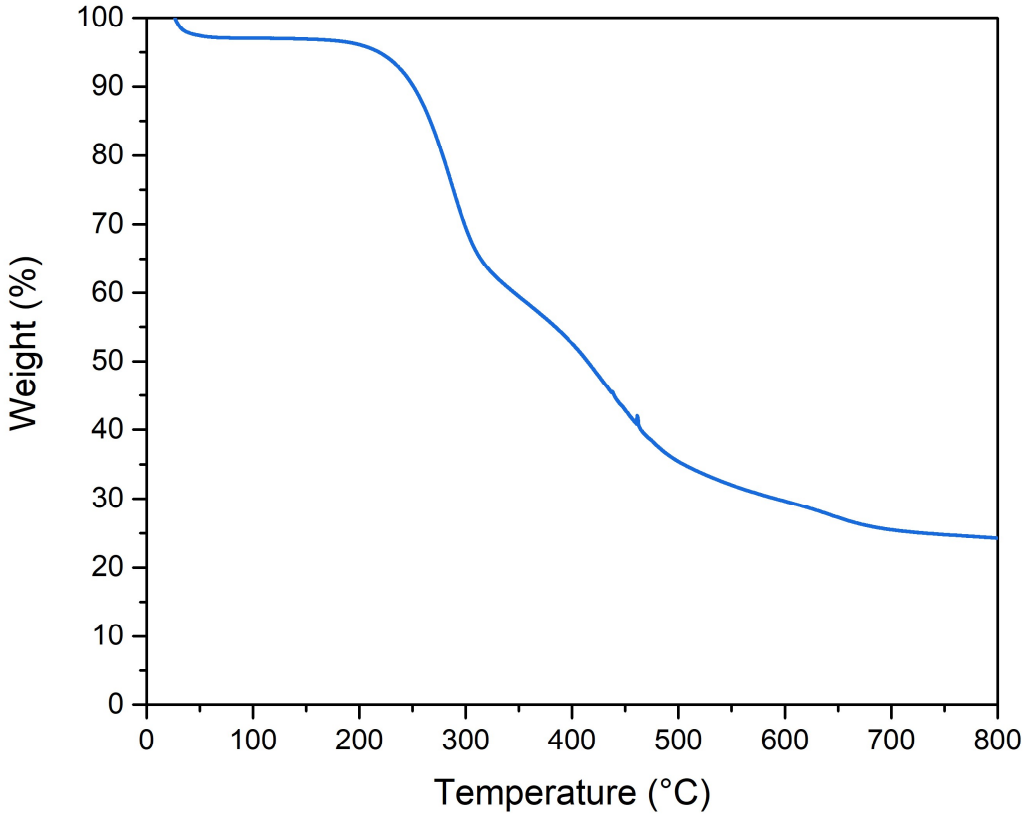

Fig. S15. TGA trace of COF-609 measured under a continuous flow of N_2. No significant weight loss was observed up to around 200 °C.

Section S6. Single-Component Sorption Experiments

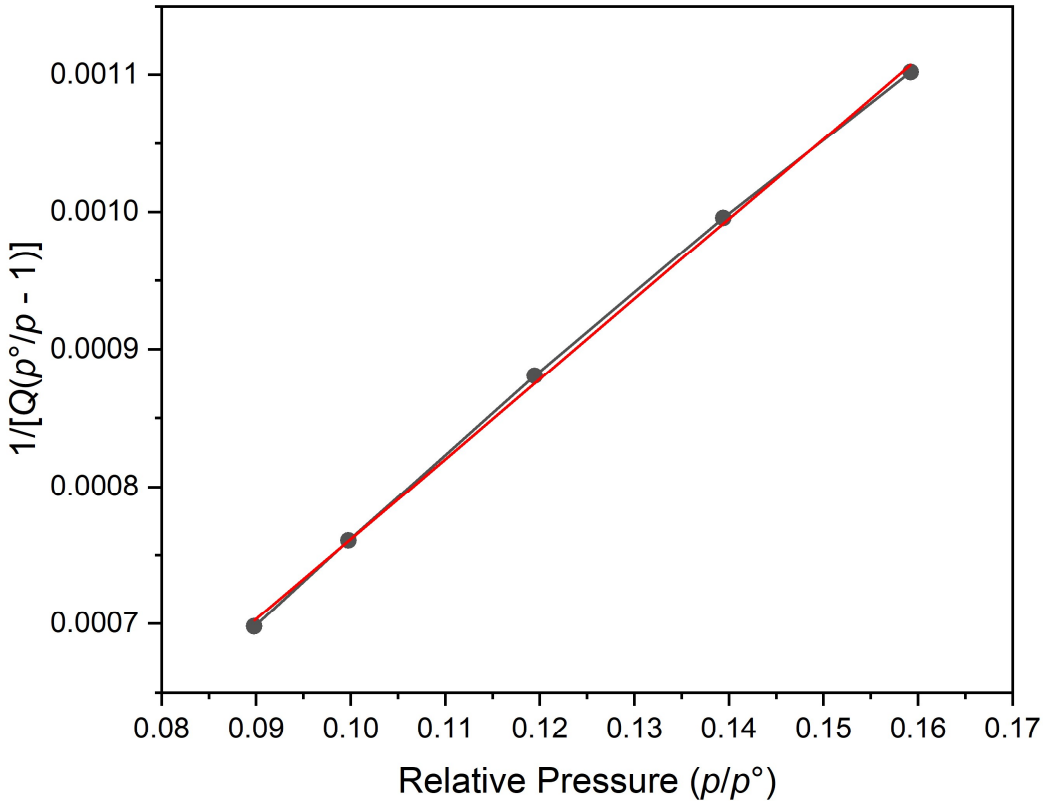

Figure S16. Brunauer-Emmett-Teller plot (black dots) and linear fitting (red line) of N_2 sorption isotherm of COF-609-Im measured at 77 K. Correlation coefficient (r) = 0.9995.

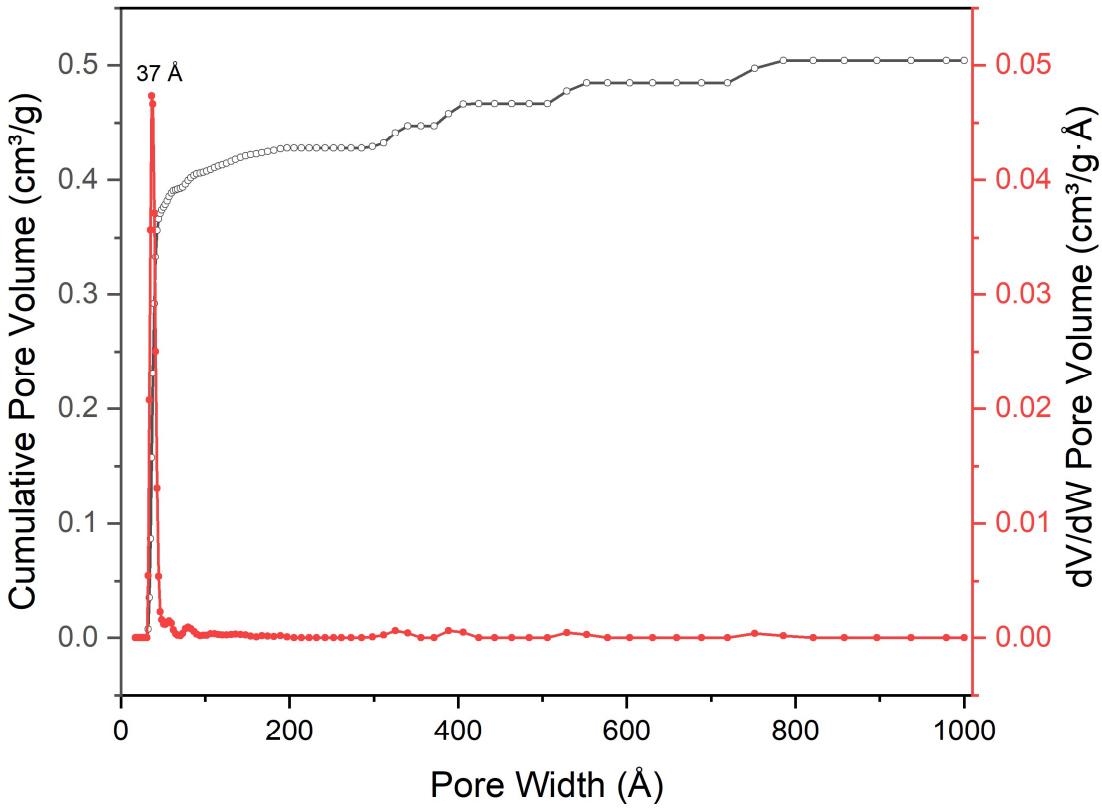

Figure S17. Pore size distribution of COF-609-Im derived from fitting its entire N_2 isotherm measured at 77 K using non-local density functional theory method, employing an N2@77-Carb Cyl Pores, MWCT model in cylindrical geometry, a regularization of 0.10000, and version 2 deconvolution, resulting in an RMS error of fit of 16.20 $cm^3\ g^{-1}$.

Section S7. Solid-State Nuclear Magnetic Resonance Spectroscopy

S7.1 Solid-State ^{13}C NMR Spectra for Post-Synthetic Modifications of COFs

Imine-^{13}C-labeled COF-609-Im (COF-609-Im-^{13}C) was synthesized by reacting TFPT-^{13}C with DABA following the same preparation as COF-609-Im, which was further post-synthetically modified following the procedures provided in Section S2.3 to yield COF-609-THQ,Im-^{13}C and COF-609-^{13}C.

S7.2 Solid-State ^{13}C and ^{15}N NMR Spectra for $^{13}CO_2$ Sorption under DAC-Relevant Conditions in the Presence of Water

Amino-^{15}N-labeled COF-609 (COF-609-^{15}N) was synthesized by reacting COF-609-THQ,Im with a 30% TRPN-^{15}N solution in unlabeled TRPN following the same reaction, workup, and activation procedure as COF-609. A fully activated COF-609-^{15}N sample was packed in an argon-filled glovebox in a breakthrough sample cell, sealed, and quickly transferred to a home-built dynamic breakthrough instrument (see details in Section S8) thoroughly flushed with a dry flow of air (ultra-zero grade, 0 ppm CO_2) overnight before loading. The sample was then treated with a 50 mL/min N_2 flow with 50% relative humidity (RH) at 1 atm and 25 °C. After saturation, to the upstream flow was continuously injected $^{13}CO_2$ at 1 atm in a gastight glass syringe (Hamilton) equipped with a PTFE septum, and at a constant rate controlled by a Chemyx Fusion 100 syringe pump through a customizable gas inlet, such that the sample was treated in a flow of ~50 mL/min 400 ppm $^{13}CO_2$ balanced in N_2 with 50% RH and at 1 atm and 25 °C until full saturation. The sample was quickly packed in air (~400 ppm CO_2, ~50% RH at ~25 °C) before submitting to the spectrometers for measurements.

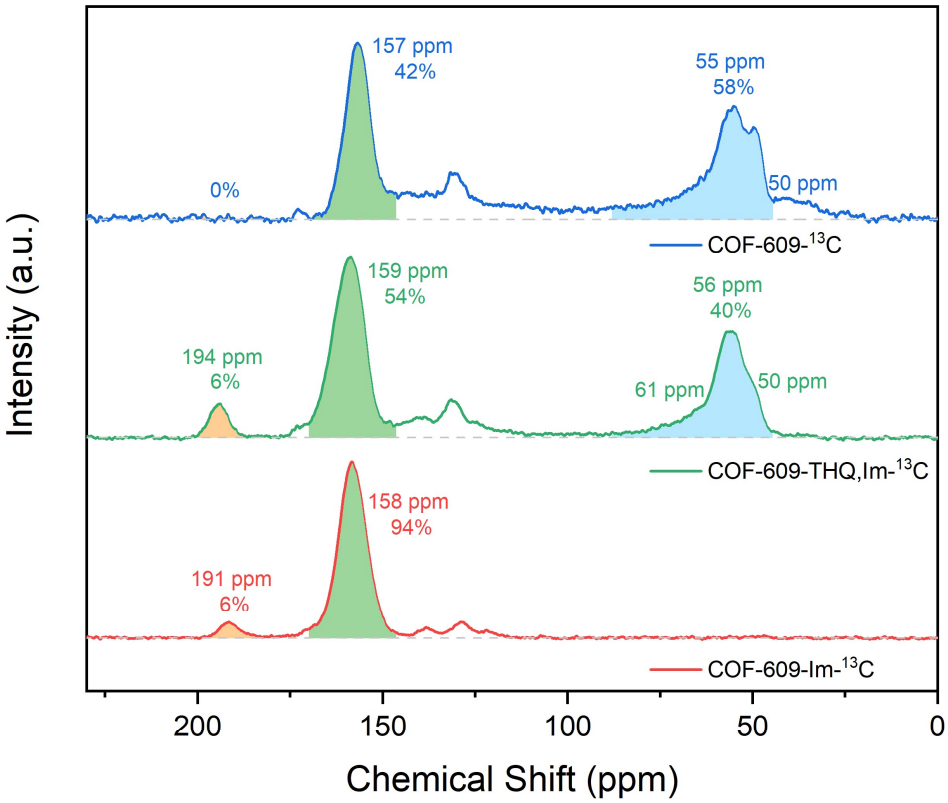

Figure S18. MultiCP/MAS solid-state ^{13}C NMR results of COF-609-Im-^{13}C, COF-609-THQ,Im-^{13}C, and COF-609-^{13}C. Colored area indicate the integration used for composition estimation in each state of conversions.

Section S8. Dynamic Breakthrough

Dynamic breakthrough and isotope-labeled gas dosing experiments (see Section S7) were conducted on a custom-built dynamic breakthrough instrument. The instrument was built based on mass balance principle, and is capable of reproducibly mixing, humidifying, contacting sample, and real-time analysis of gas-phase concentrations of CO_2 and H_2O.[7–9]

Ultra-zero grade air (0 ppm CO_2, Praxair) was first separated in two stream regulated through MFCs, where one was passed through to a saturator cell (Glassblowers) filled with deionized water and remixed with the other, in addition to another stream of 1000 ppm CO_2 balanced in air (Praxair) regulated by MFC. The mixed streams passed through a normally-closed gas injection port, a pressure sensor (Cole Parmer), and a sample/bypass gasline controlled by three solenoid valves (Parker). The flow-through quartz sample cell was filled with clean glass beads (2 mm) and glass wool to minimize dead spaces, and was soaked in a dry well (Fluke) at a controlled temperature, which was measured real-time by a thermocouple (EIC). The stream passed through a CO_2/H_2O analyzer (LICOR) before reaching a pressure controller (MKS) and lab exhaust (Figure S19).

In a typical experiment, an oven-dried flow-through cell was first filled with glass beads and glass wool was first dosed with a stream of air (0 ppm CO_2) with the desired humidity until saturation, and was then exposed to 400 ppm CO_2 balanced in air at the same humidity until saturation to measure the background uptake. This was achieved through numerical integration of the whole process, taking into account real-time fluctuations of flow and temperature compensation. The sample was then loaded to the cell an Ar filled glovebox with the same filling materials, and repeated this process to obtain an apparent uptake. The specific CO_2 uptake of the sample was then obtained as the difference between the apparent and background uptakes per unit mass of the sample.

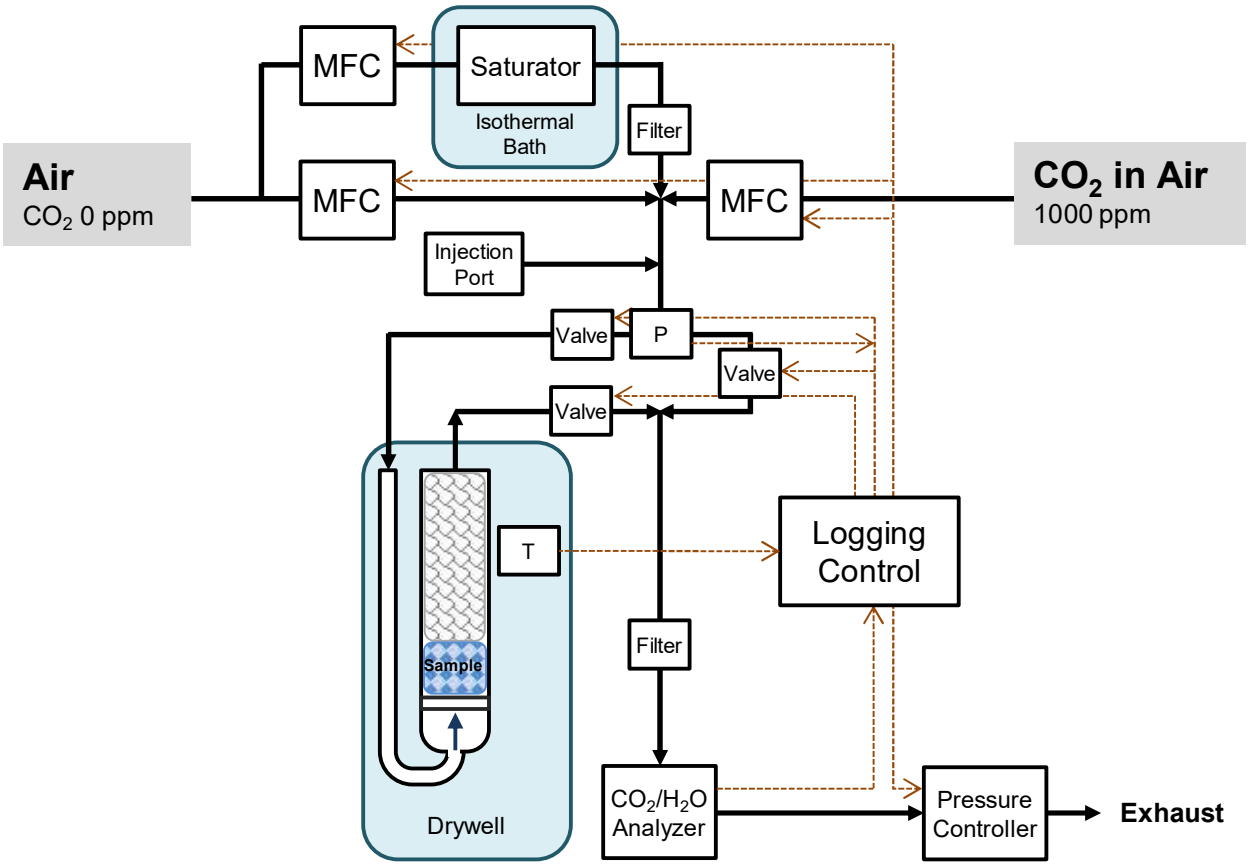

Figure S19. Device diagram of the custom-built dynamic breakthrough system. Black solid arrows indicate flow of gas streams, while brown dashed lines indicate data flow for logging or control.

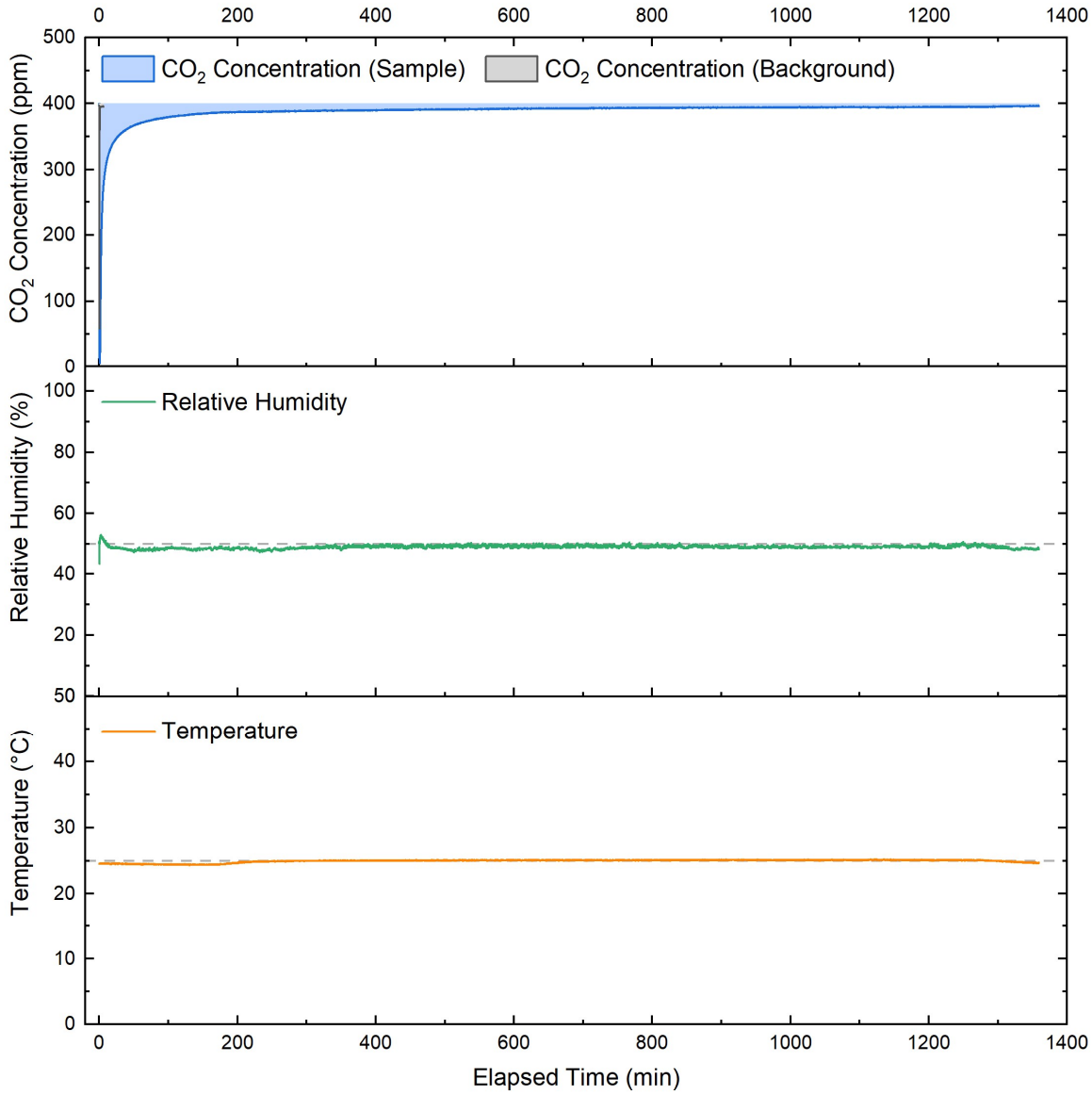

Figure S20. Breakthrough data of COF-609. In the first subplot, the area marked in blue was used for deriving the sample CO_2 uptake and background through numerical integration.

References

(1) Grunenberg, L.; Savasci, G.; Terban, M. W.; Duppel, V.; Moudrakovski, I.; Etter, M.; Dinnebier, R. E.; Ochsenfeld, C.; Lotsch, B. V. Amine-Linked Covalent Organic Frameworks as a Platform for Postsynthetic Structure Interconversion and Pore-Wall Modification. *J. Am. Chem. Soc.* **2021**, *143* (9), 3430–3438. DOI: 10.1021/jacs.0c12249.

(2) Papmeyer, M.; Vuilleumier, C. A.; Pavan, G. M.; Zhurov, K. O.; Severin, K. Molecularly Defined Nanostructures Based on a Novel AAA–DDD Triple Hydrogen-Bonding Motif. *Angew. Chem. Int. Ed.* **2016**, *55* (5), 1685–1689. DOI: 10.1002/anie.201510423.

(3) Bagchi, P.; Morgan, M. T.; Bacsa, J.; Fahrni, C. J. Robust Affinity Standards for Cu(I) Biochemistry. *J. Am. Chem. Soc.* **2013**, *135* (49), 18549–18559. DOI: 10.1021/ja408827d.

(4) Ueda, T.; Kobayashi, S. Bis (Guanidinoethyl) Amine Derivatives. *Chem. Pharm. Bull. (Tokyo)* **1969**, *17* (6), 1270–1276. DOI: 10.1248/cpb.17.1270.

(5) Kolomiĭtsova, T. D.; Kondaurov, V. A.; Sedelkova, E. V.; Shchepkin, D. N. Isotope Effects in the Vibrational Spectrum of the SF_6 Molecule. *Opt. Spectrosc.* **2002**, *92* (4), 512–516. DOI: 10.1134/1.1473589.

(6) BIOVIA, D. S. *BIOVIA Materials Studio*; Dassault Systèmes: San Diego, 2018.

(7) Nguyen, N. T. T.; Furukawa, H.; Gándara, F.; Nguyen, H. T.; Cordova, K. E.; Yaghi, O. M. Selective Capture of Carbon Dioxide under Humid Conditions by Hydrophobic Chabazite-Type Zeolitic Imidazolate Frameworks. *Angew. Chem. Int. Ed.* **2014**, *53* (40), 10645–10648. DOI: 10.1002/anie.201403980.

(8) Flaig, R. W.; Osborn Popp, T. M.; Fracaroli, A. M.; Kapustin, E. A.; Kalmutzki, M. J.; Altamimi, R. M.; Fathieh, F.; Reimer, J. A.; Yaghi, O. M. The Chemistry of CO2 Capture in an Amine-Functionalized Metal-Organic Framework under Dry and Humid Conditions. *J. Am. Chem. Soc.* **2017**, *139* (35), 12125–12128. DOI: 10.1021/jacs.7b06382.

(9) Lyu, H.; Chen, O. I.-F.; Hanikel, N.; Hossain, M. I.; Flaig, R. W.; Pei, X.; Amin, A.; Doherty, M. D.; Impastato, R. K.; Glover, T. G.; Moore, D. R.; Yaghi, O. M. Carbon Dioxide Capture Chemistry of Amino Acid Functionalized Metal–Organic Frameworks in Humid Flue Gas. *J. Am. Chem. Soc.* **2022**, *144* (5), 2387–2396. DOI: 10.1021/jacs.1c13368.